

PARP2 deficiency affects invariant-NKT,-cell maturation and protects mice from ,Concanavalin A-induced liver injury.

Aveline Filliol, Claire Piquet-Pellorce, Sarah Dion, Valentine Genet, Catherine Lucas-Clerc, Françoise Dantzer, Michel Samson

▶ **To cite this version:**

Aveline Filliol, Claire Piquet-Pellorce, Sarah Dion, Valentine Genet, Catherine Lucas-Clerc, et al.. PARP2 deficiency affects invariant-NKT,-cell maturation and protects mice from ,Concanavalin A-induced liver injury.. AJP - Gastrointestinal and Liver Physiology, 2017, 313 (5), pp.G399-G409. 10.1152/ajpgi.00436.2016 . hal-01630440

HAL Id: hal-01630440

https://univ-rennes.hal.science/hal-01630440

Submitted on 7 Nov 2017

HAL is a multi-disciplinary open access archive for the deposit and dissemination of scientific research documents, whether they are published or not. The documents may come from teaching and research institutions in France or abroad, or from public or private research centers.

L'archive ouverte pluridisciplinaire **HAL**, est destinée au dépôt et à la diffusion de documents scientifiques de niveau recherche, publiés ou non, émanant des établissements d'enseignement et de recherche français ou étrangers, des laboratoires publics ou privés.

PARP2 deficiency affects invariant-NKT-cell maturation and protects mice from Concanavalin A-induced liver injury.

Aveline Filliol[1,2,3], Claire Piquet-Pellorce[1,2,3], Sarah Dion[1,2,3], Valentine Genet[1,2,3], Catherine Lucas-Clerc[2,4], Françoise Dantzer[5], and Michel Samson[1,2,3].

[1]Institut National de la Santé et de la Recherche Médicale (Inserm), U.1085, Institut de Recherche Santé Environnement et Travail (IRSET), F-35043 Rennes, France.

[2]Université de Rennes 1, F-35043 Rennes, France.

[3]Structure Fédérative BioSit UMS 3480 CNRS-US18 Inserm, F-35043 Rennes, France.

[4]Service de Biochimie CHU Rennes, Université de Rennes 1; F-35043 Rennes, France.

[5]Université de Strasbourg, Biotechnologie et Signalisation Cellulaire, UMR7242 CNRS, Laboratoire d'Excellence Medalis, ESBS, 300, Boulevard Sébastien-Brant, CS 10413, 67412 Illkirch, France.

Correspondence: Michel Samson, INSERM-U1085, IRSET, Université de Rennes 1, 2, Avenue du Professeur Léon Bernard, 35043 RENNES Cedex, France. Phone (+33) 22 323 5927 ; Fax (+33) 22 323 4794.

Number of figures: 6

Number of tables: 1

Financial support: This work was supported by INSERM, the Ministère de

l'Education Nationale, de l'Enseignement Supérieur et de la Recherche, the Université de Rennes 1, the Région Bretagne, the "Ligue Contre le Cancer, Comités du Grand Ouest".

Conflict of interest: The authors declare no financial or commercial conflict of interest.

Keywords: Hepatitis, Parp, Liver, NKT cells, Autoimmune hepatitis

List of abbreviations:

α-GalCer: α-Galactosylceramide, ConA: Concanavalin A, DAMPs: Damage Associated Molecular Patterns, DN: double negative, DR: death receptors, NKT: Natural Killer-T, NK: Natural Killer, PARP: poly(ADP) ribose polymerase.

a. Conflict of interest.

Aveline Filliol declares no financial or commercial conflict of interest.
Claire Piquet-Pellorce declares no financial or commercial conflict of interest.
Sarah Dion declares no financial or commercial conflict of interest.
Valentine Genet declares no financial or commercial conflict of interest.
Catherine Lucas-Clerc declares no financial or commercial conflict of interest.
Françoise Dantzer declares no financial or commercial conflict of interest.
Michel Samson declares no financial or commercial conflict of interest.

b. Authors' contributions

Aveline Filliol : acquisition of data; analysis and interpretation of data, statistical analysis, drafting of the manuscript

Claire Piquet-Pellorce : acquisition of data, analysis and interpretation of data

Sarah Dion : acquisition of data, analysis and interpretation of data

Valentine Genet : acquisition of data and analysis

Catherine Lucas-Clerc : obtained technical or material support

Françoise Dantzer: drafting of the manuscript, critical revision of the manuscript for important intellectual content

Michel Samson: acquisition of data, analysis and interpretation of data, statistical analysis, drafting of the manuscript, study concept and design, study supervision

Abstract (202 words)

Excessive or persistent inflammation and hepatocyte death are the key triggers of liver diseases. The poly(ADP-ribose) polymerase (PARP) proteins induce cell death and inflammation. Chemical inhibition of PARP activity protects against liver injury during Concanavalin A (ConA)-induced hepatitis. In this mice model, ConA activates immune cells which promote inflammation and induce hepatocyte death, mediated by the activated invariant NKT-(iNKT) lymphocyte population. We analyzed immune cell populations in the liver and several lymphoid organs such as spleen, thymus, and bone marrow in *Parp2* deficient mice to better define the role of PARP proteins in liver immunity and inflammation at steady state and during ConA-induced hepatitis. We show that *i)* the genetic inactivation of *Parp2*, but not *Parp1*, protected mice from ConA hepatitis without deregulating cytokine expression and leucocyte recruitment; *ii)* cellularity was lower in the thymus, but not in spleen, liver, or bone marrow of *Parp2*$^{-/-}$ mice; *iii)* spleen and liver iNKT lymphocytes, as well as thymic T and NKT lymphocytes were reduced in *Parp2* knockout mice. In conclusion, our results suggest that the defect of T-lymphocyte maturation in *Parp2* knockout mice leads to a systemic reduction of iNKT cells, reducing hepatocyte death during ConA-mediated liver damage, thus protecting the mice from hepatitis.

INTRODUCTION

Hepatitis can be caused by various insults such as alcohol, a high fat diet, food-derived toxins, or infections, and is characterized by hepatocyte death and inflammation (5). Acute hepatitis is associated with massive hepatolysis which can lead to liver failure, whereas in chronic hepatitis, unresolved hepatolysis triggers the release of Damage Associated Molecular Patterns (DAMPs) which promote inflammation. This process induces an inflammation and cell death amplification loop that contributes to the progression of liver diseases (5, 18). Blocking the pro-inflammatory hepatocyte death response could be beneficial to in treating liver diseases.

During viral or auto-immune hepatitis, innate and adaptive lymphocytes kill hepatocytes which present proteins recognized as non-self-antigens, by the activation of death receptors (DR). In mice, Concanavalin A (ConA)-induced liver injury mimics immune cell-mediated hepatitis in humans (27) and is dependent on innate Natural Killer T (NKT) lymphocytes. NKT cells are involved in numerous immune responses and are particularly abundant in the liver and spleen of mice. They have the ability to recognize lipids presented by CD1d which allows there distinction into two categories of NKT cells. Type I or invariant-NKT (iNKT) cells express an invariant T-cell receptor α-chain (TCRα; Vα14-Jα18) and are able to recognize the α-Galactosylceramide (α-GalCer) presented by CD1d. Type II NKT cells express more diverse TCR Vα chains that cannot recognize α-GalCer and are characterized as CD4/CD8 double negative (DN). The iNKT are the major NKT subset in the liver and $CD1d^{-/-}$ (NKT deficient) mice as well as $V\alpha14^{-/-}$ (iNKT deficient) mice are protected from ConA-induced hepatitis (15, 26-28). ConA activates liver immune cells which promote hepatocyte death in two ways. First, activated immune

cells release large amounts of cytokines, such as TNF-α (17, 21), IFN-γ (12, 25) and IL-4 (13) which play key roles in the hepatocyte death process (17, 27, 29). Second, activated NKT cells, potent producers of IFN- γ, kill hepatocytes by activation of the TNF-superfamily DR (3, 23, 26, 33) and the perforin/granzyme B system (31). Our group has extensively investigated the mechanisms of hepatocyte death during hepatitis. We and others have demonstrated a key role for PARP proteins in the liver. We have shown that inhibition of poly(ADP) ribose polymerase (PARP) 1 and 2 activity with the PJ-34-inhibitor protects mice from ConA-mediated hepatolysis (2, 14). Mukhopadhyay *et al.* have shown that genetic or chemical inhibition of PARP1 also prevents liver inflammation and fibrosis induced by the hepatotoxic carbon tetrachloride (CCl4) or bile duct ligation (22). PARP1 and PARP2 are activated by DNA strand breaks and use NAD^+ as a substrate to synthetize chains of poly(ADPribose) onto various acceptor proteins, thereby inducing chromatin remodeling and the recruitment of DNA repair complexes (8). In the last decades, PARP1 and PARP2 have also been found to play an important role in inflammation (4) and cell death (30). In this study, we aimed to better define the roles of PARP1 and PARP2 proteins in ConA-induced hepatitis using the *Parp1* and *Parp2* knockout mouse models.

METHODS

Animals and treatment protocols

C57BL/6 *Parp1* and *Parp2* genetically modified mice (*Parp1*$^{-/-}$ and *Parp2*$^{-/-}$, respectively) were provided by Dr. F. Dantzer and generated as described previously (7, 32). Heterozygous mice were crossed to obtain knockout and littermate WT mice. Adult male and female mice, of 10 to 12 weeks of age, were used for each

experiment with the ConA model. ConA (C2010 Sigma-Aldrich, St. Louis, MO) was prepared at 3 mg/mL in PBS supplemented with 0.31 mM $MnCl_2$ and 0.75 mM $CaCl_2$ and administered by intravenous (i.v.) injection at a dose of 10 or 12 mg/kg body weight. For histopathological and biochemical studies, mice treated with ConA were compared to mice which received PBS supplemented with 0.31 mM $MnCl_2$ and 0.75 mM $CaCl_2$. For all phenotypic immune cell analyses, adult (10 to 12 weeks old) or early adult (five- week-old) mice were either not treated, to analyze the population at steady state, or treated with ConA. Animals were housed in individual cages and bred in specific pathogen-free conditions in the local animal house facilities. All treatment protocols were in accordance with the French laws and the institution's guidelines for animal welfare (agreement of M. Samson # R-2012-CPP-01).

Histopathological and biochemical studies

Mouse liver biopsies were fixed in 4% paraformaldehyde and embedded in paraffin for IHC and hematoxylin and eosin (H&E) staining. For histopathology, H&E staining of liver tissues was carried out to investigate liver injury. Serum ALT and AST transaminases were measured according to the IFCC primary reference procedures using an Olympus AU2700 Autoanalyser® (Olympus Optical, Tokyo, Japan).

RNA analysis

Total RNA was extracted from mouse livers using TRIzol reagent (Invitrogen). First-strand cDNA was synthesized using the SuperScript™ II Reverse Transcriptase (Invitrogen). Real-time quantitative PCR was performed using the fluorescent dye

SYBR Green with the double-strand specific SYBR® Green system (Applied Biosystems) and the ABI 7000 Prism sequence detector (Applied Biosystems) or the CFX384 Touch™ Real-Time PCR Detection System (Bio-Rad). cDNA was used as template for amplification using specific primer pairs (Table 1). Each measurement was performed in triplicate. The relative gene expression was normalized against 18S rRNA gene expression. The control mice in each treatment group served as a reference for messenger RNA (mRNA) expression (the control mRNA level was arbitrarily set to 1).

Immune cell analysis by flow cytometry

Immune cells were prepared from spleen, thymus, or liver crushed on a 70 µm filter. Liver immune cells were isolated after sedimentation and cell fractionation on a 35% Percoll layer. For each organ, red blood cells were lysed using ammonium-chloride-potassium (ACK) buffer. Bone marrow immune cells were isolated by flushing two femurs with RPMI medium (Gibco). The number of immune cells was determined by counting in a Malassez counting chamber.

Cell suspensions were labeled for 30 min with LIVE/DEAD fixable yellow stain (Life technologies, L34959) to exclude dead cells from the analysis. Cells were also pre-incubated with an anti-CD16/32 antibody (BD Pharmingen) to block non-specific binding before incubation with the appropriate fluorochrome-conjugated antibodies (BD Pharmingen, eBioscience): anti-CD3-FITC (clone 17A2), anti- TCRβ-V450 (clone H57-597), anti-CD69-PE (clone H1.2F3), anti-CD19-APC or anti-CD19-PE (clone 1D3), anti-NK1.1-PerCP-Cy-5.5 (clone PK136), anti-CD4-PE-Cy7 (clone RM4-5), anti-CD8-APC-Cy7 (clone 53-6.7), anti-GR1-eFluor450 (clone FB6-8C5), anti-

CD11b-PE-Cy7 (clone M1/70), anti-Sca1-PE (clone D7), anti-c-kit-PerCP-eFluor710 (clone 2B8), anti-Ter119-eFluor780 (clone Ter119), and empty CD1d tetramer or CD1d tetramer loaded with α- galactosylceramide (GalCer)-PE (provided by Dr. M. Leite de Morales). The stained cells were analyzed on a FACSAria™ II flow cytometer and data were analyzed using CXP software (Beckman Coulter). Doublets and dead cells were excluded on the basis of forward/side scatter and LIVE/DEAD labeling, respectively. The immuno-phenotyping used was as follows: B-lymphocytes: CD19+/CD3- cells; T-lymphocytes: CD3+/TCRVβ+/NK1.1-; NKT cells: CD3+/TCRVβ+/NK1.1+; NK cells: CD3-/NK1.1+; and granulocytes: GR1+CD11b+. Lymphoid activation was studied by analyzing the expression of CD69. We calculated the percentage of each immune cell population, by considering the sum of events of all immune cell populations analyzed (sum of T, NK, NKT, B cells and myeloid cells) as 100% of the total immune cells. The absolute number in each immune cell population was calculated by multiplying the percentage of each population by the total number of immune cells.

Serum cytokine immunoassay by flow cytometry

Murine TNF-α, IFN-γ and IL-6 cytokines were quantified by bead-based immunoassays according to manufacturer protocol, using a filter plate and a vacuum filtration system for washing steps (BioLegend's LEGENDPLEX, multi-analyte flow assay kit). Samples were analyzed on a LSR Fortessa cytometer (BD Biosciences).

Statistical analysis

Data are expressed as the means +/- SEM for all mice treated similarly. Kruskal–Wallis one-way analysis of variance (ANOVA) was performed, and mean differences between experimental groups were assessed using the non-parametric Mann–Whitney *U*-test using GraphPad Prism5 software.

RESULTS

PARP2 but not PARP1 deficiency protects mice from ConA-induced hepatitis

We investigated the role of PARP1 and PARP2 proteins in hepatitis using adult knockout mice for PARP1 (*Parp1*$^{-/-}$) and PARP2 (*Parp2*$^{-/-}$) and comparing the results to those obtained using wild-type mice (WT). We challenged mice with ConA to induce hepatitis, or with PBS as a control, and evaluated liver damage using serum transaminase (ALT and AST) levels and hematoxylin coloration. In ConA induced-hepatitis, the peak of hepatolysis occurs 11 h after ConA treatment.(29) *Parp1*$^{-/-}$ mice displayed visibly, but non-significantly, lower ALT and AST transaminase levels than WT mice at this time point. In contrast, *Parp2*$^{-/-}$ mice were highly protected from ConA-induced hepatitis as they had significantly lower (4-fold) levels of both AST and ALT than WT mice (Fig. 1A). Accordingly, H&E coloration of liver slides from Con A-treated WT and *Parp2*$^{-/-}$ mice, revealed fewer areas of necrosis in *Parp2* deficient mice than in WT mice (Fig. 1B). Moreover, the absence of PARP2 appeared to protect mice from hepatolysis and did not simply delay liver injury as serum transaminase levels remained significantly lower in *Parp2*$^{-/-}$ mice than in WT mice, even 24 h after ConA administration (Fig. 1C). We next evaluated the level of inflammation induced by ConA, by measuring the mRNA levels of TNF-α, IFN-γ, IL-1β, and IL-4, all known to play key roles during ConA-induced hepatitis. TNF-α, IFN-

γ, IL-1β, and IL-4 transcript levels were higher in all genotypes after ConA treatment. However, we observed no significant differences between the IFN-γ or IL-4 mRNA levels in *Parp1*$^{-/-}$, *Parp2*$^{-/-}$, or WT mice, whereas TNF-α transcript levels were significantly lower in *Parp2*$^{-/-}$ mice than in the other two mouse strains. In contrast, IL-1β mRNA levels were higher in both *Parp2*$^{-/-}$ and *Parp1*$^{-/-}$ mice than in WT mice. Next, we analyze serum cytokines from WT and Parp2-/- mice. TNF-α, IFN-γ and IL-6 were up-regulated in both genotypes after ConA challenge. However, TNF-α and IFN-γ levels were similar between WT and Parp2-/- mice, whereas IL-6 rate decreased in Parp2-/- mice (Fig. 1E).

Parp2$^{-/-}$ mice display a substantial reduction in the number of liver iNKT cells

We performed all further experiments using only the *Parp2*$^{-/-}$ mouse model, as PARP2 protein deficiency protected mice from ConA-induced liver damage, whereas that of PARP1 did not. ConA induces liver injury in an immune cell-dependent manner. Thus we next measured the steady-state, basal levels of the different liver immune cell subsets in *Parp2*$^{-/-}$ mice of two different ages: early adult (five weeks) and adult (10 to 12 weeks) by flow cytometry. Cell doublets and dead cells were excluded and the phenotypic analysis of liver immune cells was determined using the gating strategy presented in Figure 2A.

Parp2$^{-/-}$ mice displayed a similar number of liver immune cells as WT mice at the two different ages (Fig. 2B). The absolute number of total T lymphocytes and the ratio of CD4:CD8 T-lymphocytes were also similar in the livers of both genotypes (Fig. 2C). We next analyzed the NKT-lymphocyte population, defined as CD3, TCRVβ, and NK1.1 positive cells. We used the CD1d tetramer loaded with αGalCer to analyze the invariant-NKT (iNKT) subset (CD3+ TCRVβ+ NK1.1+ αGalCer+) and the anti-CD4

antibody to study NKT DN cells (CD3+ TCRVβ+ NK1.1+ αGalCer- CD4-). *Parp2*$^{-/-}$ mice displayed a reduction in the percentage of total liver NKT cells of two fold in five-week-old mice and of 1.5 fold in 10-12-week-old mice (Fig. 2D). However, PARP2 deficiency did not impair the increase in the percentage of liver NKT cells as the mice aged (Fig 2D). We also observed that only the percentage of iNKT cells, but not NKT DN cells, was significantly lower in the *Parp2*$^{-/-}$ mice at both ages (Fig. 2E). The absolute number of liver immune cells was similar between both genotypes, whereas the number of iNKT cells was lower in *Parp2*$^{-/-}$ mice. We thus aimed to determine which immune cell subsets compensated this reduction. The percentage of NK-cells (NK1.1+ CD3-) and B-lymphocytes (CD19+ CD11b-) were higher in five-week-old *Parp2*$^{-/-}$ mice, but only the percentage of NK-cells was higher in adult Parp2 $^{-/-}$ mice (Fig. 2F and 2G). The liver myeloid compartment, based on GR1 and CD11b labelling, also appeared to be similar in *Parp2*$^{-/-}$ and WT mice, regardless of age (Fig. 2H). In conclusion, PARP2 deficiency induced a significant reduction in the number of iNKT cells in the liver which was not compensated by an increase of all immune cell subsets, but by a gain of B and NK-lymphocytes.

PARP2 deficiency does not affect the recruitment and activation of immune cells during ConA-induced hepatitis.

We next examined the impact of PARP2 deficiency on ConA-induced cell recruitment and activation. ConA-induced inflammation and cell death induced a similarly high level of leucocyte recruitment to the liver in mice of both genotypes as seen by the large increase in the absolute number of liver immune cells 11 h after injection, which then decreased with the resolution of the hepatitis 24 h after ConA treatment (Fig. 3A). We evaluated the NKT-cell subset and found a reduction in the number of NKT

cells in the livers of mice of both genotypes upon ConA treatment. However, this reduction was 3.7 fold in WT mice, relative to untreated mice, but only 1.7 fold in *Parp2*$^{-/-}$ mice, (Fig. 3B). The absence of PARP2 protein did not seem to affect the recruitment of other leucocyte populations, as T, B, and NK-lymphocytes, and myeloid cells were similarly recruited for both genotypes 11 h after ConA administration (Fig. 3C). Finally, we analyzed the early activation marker CD69 on lymphocytes and observed that more than 90% of T-lymphocytes in both *Parp2*$^{-/-}$ and WT mice were activated after ConA treatment (Fig. 3D).

Parp2$^{-/-}$ mice have fewer spleen iNKT cells than WT mice

We demonstrated that *Parp2*$^{-/-}$ mice were protected from ConA-hepatitis and had fewer hepatic NKT cells, without affecting ConA-induced inflammation. We next analyzed the immune cell subsets in the various lymphoid compartments such as spleen, bone marrow, and thymus. Gating strategies used for splenocyte analysis are depicted in Supplementary Figures 1 and 2. PARP2 deficiency did not affect the absolute number of splenocytes in mature mice but they were slightly, but not significantly, higher in number in early adult mice (Fig. 4A). We then evaluated the percentage cells in each immune cell subset in the spleen. The number of T-lymphocytes (CD3+ NK1.1- TCRVβ+) were lower only in early adult *Parp2*$^{-/-}$ mice (Fig. 4B) and was compensated by an increase in the number of B-lymphocytes (CD19+ CD11b-) (Fig. 4C). Similar to our observations in the liver, the spleens of five- and 10-12-week-old *Parp2*$^{-/-}$ mice had significantly fewer NKT cells than those of WT mice, and only the iNKT cells were affected (Fig. 4D). In contrast to the liver, the number of spleen NK cells was only slightly, but not significantly, higher in Parp2 $^{-/-}$ than in WT mice (Fig. 4E).

Parp2$^{-/-}$ mice have fewer thymus iNKT cells than WT mice.

We next investigated the thymocyte population of five-week-old mice to understand the cause of the reduction in NKT-cell number in the liver and spleen of *Parp2*$^{-/-}$ mice. The absolute number of thymocytes was lower in *Parp2*$^{-/-}$ mice than in WT mice, and was associated with a reduction in the absolute number of immature CD4/CD8 double positive (DP) and CD4 or CD8 simple positive (SP) thymocytes (Fig. 5A and 5B). The absolute number of iNKT cells (αGalCer^{+}) was also lower in *Parp2*$^{-/-}$ mice (Fig. 5C). However, the remaining iNKT cells expressed wild-type levels of mature T lymphocyte markers such as CD3 and TCRVβ (Fig. 5D).

Parp2$^{-/-}$ mice have more Ter119^{+}-cells than WT mice.

Finally, we eliminated doublets and dead cells, analyzed BM immune cells by flow cytometry to analyze the different immune cell subsets, as depicted in Figure 3A, then we investigated the immune cell subsets in the bone marrow (BM) of *Parp2*$^{-/-}$ mice. As observed in the spleen and the liver, BM cellularity was similar between *Parp2*$^{-/-}$ and WT adult mice (Fig. 6B). The absolute numbers of the different mature BM cell subsets (CD19+, GR1high CD11b+, GR1high CD11b+ and CD3^{+}) were similar with slight variations between the two genotypes, except for Ter119 positive cells which were significantly more numerous in *Parp2*$^{-/-}$ mice (Fig. 6C). Similarly, the number of Lin^{-} cells (Ter119- CD19- CD3- GR1- CD11b-) was slightly, but not significantly higher in the *Parp2*$^{-/-}$ mice, and was associated with a small increase in the number of the myeloid progenitor (MP) (Lin- ckit+ Sca-) and LSK populations (Lin- ckit+ Sca+) (Fig. 6D).

DISCUSSION

We previously reported that inhibition of PARP protein activity with the PJ-34 inhibitor protected mice from ConA-induced hepatolysis (2, 14). PARP proteins mediate the activation of various transcription factors, such as NF-κB, to promote inflammation in several inflammatory diseases, including CCl4 induced chronic liver injury. Inactivation or inhibition of PARP proteins prevents inflammation-induced tissue damage (4). Inflammation induced by ConA plays a key role in the induction of hepatolysis (12, 13, 17, 21, 25). However, we previously demonstrated that PJ-34 does not inhibit inflammation during ConA-induced hepatitis, as cytokine release and liver leucocyte recruitment occurred efficiently, suggesting a more direct role for PARP proteins in the induction of hepatocyte death (2, 14). Here, we show that the genetic inactivation of *Parp2*, but not *Parp1*, protects mice from ConA-induced hepatitis without deregulating inflammation, as leucocyte recruitment and pro-inflammatory cytokine expression were not affected. Analysis of liver and spleen immune populations revealed a substantial reduction in the percentage of iNKT cells, normally enriched in both organs (19). The reduction in the number of iNKT in *Parp2*$^{-/-}$ mice may explain the reduced hepatolysis and protection from ConA-induced hepatitis observed in these mice. Indeed, rapid elimination of NKT cells after ConA treatment is a marker of NKT-induced liver injury following their activation (26). We also observed the elimination of NKT cells after ConA treatment in both *Parp2*$^{-/-}$ and WT mice, but as fewer NKT cells were present in the untreated *Parp2*$^{-/-}$ mice relative to WT mice, there were fewer NKT cells available to induce hepatocyte cell death after ConA treatment in these mice. Surprisingly, whereas IFN-γ is highly produced by NKT cells, we did not observed a reduction of both its expression and its serum level in *Parp2*$^{-/-}$ mice. However in the liver, the reduction of NKT-cell number was

compensated by an increase in the number of NK cells which are potent producers of IFN-γ. As a consequence, in *Parp2*$^{-/-}$ mouse liver, the increase of NK cells could compensated the NKT-cell reduction in the inflammatory process. However, the increase in NK-cell number was not sufficient to restore hepatocyte cell death, as ConA-induced liver injury is strictly NKT-dependent and NK-independent (26, 28). Our study using *Parp1* and *Parp2* knockout mice did not allow us to clarify the effect of the PJ-34 inhibitor. Moreover, the fact that *Parp1*$^{-/-}$ mice were not protected against ConA-induced hepatitis, suggests that PARP2 participates in ConA-mediated liver injury, as the two proteins share common functions (1, 8). *Parp1* and *Parp2* double knockout mice are lethal (20). It may be informative to use conditional knockout mice to further decipher the role of both proteins in the liver.

We analyzed the thymus and bone marrow of *Parp2*$^{-/-}$ mice to identify the cause of the systemic reduction of iNKT cells detected in these mice. As previously described, *Parp2*$^{-/-}$ mice displayed an increase of the erythroid subset (10), but no T-lymphocyte deregulation. iNKT cells mature in the thymus and are derived from the DP population (11). In agreement with others, we observed a reduction in the number of DP-thymocytes in the absence of PARP2 protein (32) and revealed a substantial reduction in the number of thymic iNKT cells. PARP2 deficiency leads to inefficient Vα to Jα rearrangement inducing the death of DP-thymocytes (32), resulting in a decrease in the number of mature SP T-lymphocytes and iNKT cells. However, only iNKT-cell numbers were lower in the liver and spleens of adult mice, but not those of conventional T-lymphocytes.

The rearrangement of TCR occurs at the DP-thymocyte stage and involves DNA-break and DNA-repair mechanisms. PARP2 is sensitized to DNA damage (8) and has been highlighted to play a role in the TCRα rearrangement process during

thymocyte development, as *Parp2*$^{-/-}$ DP thymocytes display a skewed TCRα repertoire and a decrease of cell survival (32). The rearrangement of the TCRα locus occurs in a sequential manner from proximal to distal regions (16) and *Parp2*$^{-/-}$ DP-thymocytes present a reduction of the distal segments Jα42 to Jα4 (32). Interestingly, iNKT cell lineage differentiates at the DP stage and is characterized by expression of an unique TCRα chain with a Vα14-Jα18 rearrangement. As the Jα18 segment is located between the segments Jα42 and Jα4, this strongly suggests that use of Jα18 is reduced in DP-thymocyte *Parp2*$^{-/-}$, and could explain the reduction of iNKT-lymphocyte subset. This is supported by the fact that a default of TCRα rearrangement is known to induce DP-thymocyte cell death (16) and that *Parp2*$^{-/-}$ thymocytes present a shorter lifespan (32).

In conclusion, previous phenotypic investigations of *Parp2*$^{-/-}$ mice revealed an important role of the PARP2 protein in the regulation of lipid metabolism (24), erythropoiesis (9), thymopoiesis (32) and spermatogenesis (6). Here, we highlight a new phenotype in *Parp2*$^{-/-}$ mice associated with the deregulation of thymopoiesis, resulting in a systemic iNKT deficiency, leading to protection against ConA-induced liver injury.

Acknowledgements

This work was supported by INSERM, The Ministère de l'Education Nationale de la Recherche et de la Technologie, the University of Rennes 1, the Région Bretagne and the "Ligue Contre le Cancer, Comités du Grand Ouest". AF was supported by a PhD fellowship from the Région Bretagne. We would like to thank the dedicated

platforms for immunohistochemistry analysis and animal house facilities (i.e. H2P2 and animal house platforms) of SFR BIOSIT, University of Rennes 1, France.

References

1. **Ame JC, Spenlehauer C, and de Murcia G.** The PARP superfamily. *Bioessays* 26: 882-893, 2004.
2. **Arshad MI, Piquet-Pellorce C, Filliol A, L'Helgoualc'h A, Lucas-Clerc C, Jouan-Lanhouet S, Dimanche-Boitrel MT, and Samson M.** The chemical inhibitors of cellular death, PJ34 and Necrostatin-1, down-regulate IL-33 expression in liver. *J Mol Med (Berl)* 93: 867-878, 2015.
3. **Arshad MI, Piquet-Pellorce C, L'Helgoualc'h A, Rauch M, Patrat-Delon S, Ezan F, Lucas-Clerc C, Nabti S, Lehuen A, Cubero FJ, Girard JP, Trautwein C, and Samson M.** TRAIL but not FasL and TNFalpha, regulates IL-33 expression in murine hepatocytes during acute hepatitis. *Hepatology* 56: 2353-2362, 2012.
4. **Bai P and Virag L.** Role of poly(ADP-ribose) polymerases in the regulation of inflammatory processes. *FEBS Lett* 586: 3771-3777, 2012.
5. **Brenner C, Galluzzi L, Kepp O, and Kroemer G.** Decoding cell death signals in liver inflammation. *J Hepatol* 59: 583-594, 2013.
6. **Dantzer F, Mark M, Quenet D, Scherthan H, Huber A, Liebe B, Monaco L, Chicheportiche A, Sassone-Corsi P, de Murcia G, and Menissier-de Murcia J.** Poly(ADP-ribose) polymerase-2 contributes to the fidelity of male meiosis I and spermiogenesis. *Proc Natl Acad Sci U S A* 103: 14854-14859, 2006.
7. **de Murcia JM, Niedergang C, Trucco C, Ricoul M, Dutrillaux B, Mark M, Oliver FJ, Masson M, Dierich A, LeMeur M, Walztinger C, Chambon P, and de Murcia G.** Requirement of poly(ADP-ribose) polymerase in recovery from DNA damage in mice and in cells. *Proc Natl Acad Sci U S A* 94: 7303-7307, 1997.
8. **De Vos M, Schreiber V, and Dantzer F.** The diverse roles and clinical relevance of PARPs in DNA damage repair: current state of the art. *Biochem Pharmacol* 84: 137-146, 2012.
9. **Farres J, Llacuna L, Martin-Caballero J, Martinez C, Lozano JJ, Ampurdanes C, Lopez-Contreras AJ, Florensa L, Navarro J, Ottina E, Dantzer F, Schreiber V, Villunger A, Fernandez-Capetillo O, and Yelamos J.** PARP-2 sustains erythropoiesis in mice by limiting replicative stress in erythroid progenitors. *Cell Death Differ* 22: 1144-1157, 2015.
10. **Farres J, Martin-Caballero J, Martinez C, Lozano JJ, Llacuna L, Ampurdanes C, Ruiz-Herguido C, Dantzer F, Schreiber V, Villunger A, Bigas A, and Yelamos J.** Parp-2 is required to maintain hematopoiesis following sublethal gamma-irradiation in mice. *Blood* 122: 44-54, 2013.
11. **Gapin L, Matsuda JL, Surh CD, and Kronenberg M.** NKT cells derive from double-positive thymocytes that are positively selected by CD1d. *Nat Immunol* 2: 971-978, 2001.
12. **Hong F, Jaruga B, Kim WH, Radaeva S, El-Assal ON, Tian Z, Nguyen VA, and Gao B.** Opposing roles of STAT1 and STAT3 in T cell-mediated hepatitis: regulation by SOCS. *J Clin Invest* 110: 1503-1513, 2002.
13. **Jaruga B, Hong F, Sun R, Radaeva S, and Gao B.** Crucial role of IL-4/STAT6 in T cell-mediated hepatitis: up-regulating eotaxins and IL-5 and recruiting leukocytes. *J Immunol* 171: 3233-3244, 2003.
14. **Jouan-Lanhouet S, Arshad MI, Piquet-Pellorce C, Martin-Chouly C, Le Moigne-Muller G, Van Herreweghe F, Takahashi N, Sergent O, Lagadic-Gossmann D, Vandenabeele P, Samson M, and Dimanche-Boitrel MT.** TRAIL induces necroptosis involving RIPK1/RIPK3-dependent PARP-1 activation. *Cell Death Differ* 19: 2003-2014, 2012.

15. **Kaneko Y, Harada M, Kawano T, Yamashita M, Shibata Y, Gejyo F, Nakayama T, and Taniguchi M.** Augmentation of Valpha14 NKT cell-mediated cytotoxicity by interleukin 4 in an autocrine mechanism resulting in the development of concanavalin A-induced hepatitis. *J Exp Med* 191: 105-114, 2000.
16. **Krangel MS, Carabana J, Abbarategui I, Schlimgen R, and Hawwari A.** Enforcing order within a complex locus: current perspectives on the control of V(D)J recombination at the murine T-cell receptor alpha/delta locus. *Immunol Rev* 200: 224-232, 2004.
17. **Kusters S, Tiegs G, Alexopoulou L, Pasparakis M, Douni E, Kunstle G, Bluethmann H, Wendel A, Pfizenmaier K, Kollias G, and Grell M.** In vivo evidence for a functional role of both tumor necrosis factor (TNF) receptors and transmembrane TNF in experimental hepatitis. *Eur J Immunol* 27: 2870-2875, 1997.
18. **Luedde T, Kaplowitz N, and Schwabe RF.** Cell death and cell death responses in liver disease: mechanisms and clinical relevance. *Gastroenterology* 147: 765-783 e764, 2014.
19. **Matsuda JL, Naidenko OV, Gapin L, Nakayama T, Taniguchi M, Wang CR, Koezuka Y, and Kronenberg M.** Tracking the response of natural killer T cells to a glycolipid antigen using CD1d tetramers. *J Exp Med* 192: 741-754, 2000.
20. **Menissier de Murcia J, Ricoul M, Tartier L, Niedergang C, Huber A, Dantzer F, Schreiber V, Ame JC, Dierich A, LeMeur M, Sabatier L, Chambon P, and de Murcia G.** Functional interaction between PARP-1 and PARP-2 in chromosome stability and embryonic development in mouse. *EMBO J* 22: 2255-2263, 2003.
21. **Mizuhara H, O'Neill E, Seki N, Ogawa T, Kusunoki C, Otsuka K, Satoh S, Niwa M, Senoh H, and Fujiwara H.** T cell activation-associated hepatic injury: mediation by tumor necrosis factors and protection by interleukin 6. *J Exp Med* 179: 1529-1537, 1994.
22. **Mukhopadhyay P, Rajesh M, Cao Z, Horvath B, Park O, Wang H, Erdelyi K, Holovac E, Wang Y, Liaudet L, Hamdaoui N, Lafdil F, Hasko G, Szabo C, Boulares AH, Gao B, and Pacher P.** Poly (ADP-ribose) polymerase-1 is a key mediator of liver inflammation and fibrosis. *Hepatology* 59: 1998-2009, 2014.
23. **Seino K, Kayagaki N, Takeda K, Fukao K, Okumura K, and Yagita H.** Contribution of Fas ligand to T cell-mediated hepatic injury in mice. *Gastroenterology* 113: 1315-1322, 1997.
24. **Szanto M, Brunyanszki A, Marton J, Vamosi G, Nagy L, Fodor T, Kiss B, Virag L, Gergely P, and Bai P.** Deletion of PARP-2 induces hepatic cholesterol accumulation and decrease in HDL levels. *Biochim Biophys Acta* 1842: 594-602, 2014.
25. **Tagawa Y, Sekikawa K, and Iwakura Y.** Suppression of concanavalin A-induced hepatitis in IFN-gamma(-/-) mice, but not in TNF-alpha(-/-) mice: role for IFN-gamma in activating apoptosis of hepatocytes. *J Immunol* 159: 1418-1428, 1997.
26. **Takeda K, Hayakawa Y, Van Kaer L, Matsuda H, Yagita H, and Okumura K.** Critical contribution of liver natural killer T cells to a murine model of hepatitis. *Proc Natl Acad Sci U S A* 97: 5498-5503, 2000.
27. **Tiegs G, Hentschel J, and Wendel A.** A T cell-dependent experimental liver injury in mice inducible by concanavalin A. *J Clin Invest* 90: 196-203, 1992.
28. **Toyabe S, Seki S, Iiai T, Takeda K, Shirai K, Watanabe H, Hiraide H, Uchiyama M, and Abo T.** Requirement of IL-4 and liver NK1+ T cells for concanavalin A-induced hepatic injury in mice. *J Immunol* 159: 1537-1542, 1997.
29. **Trautwein C, Rakemann T, Brenner DA, Streetz K, Licato L, Manns MP, and Tiegs G.** Concanavalin A-induced liver cell damage: activation of intracellular pathways triggered by tumor necrosis factor in mice. *Gastroenterology* 114: 1035-1045, 1998.
30. **Virag L, Robaszkiewicz A, Rodriguez-Vargas JM, and Oliver FJ.** Poly(ADP-ribose) signaling in cell death. *Mol Aspects Med* 34: 1153-1167, 2013.
31. **Watanabe Y, Morita M, and Akaike T.** Concanavalin A induces perforin-mediated but not Fas-mediated hepatic injury. *Hepatology* 24: 702-710, 1996.

494 32. **Yelamos J, Monreal Y, Saenz L, Aguado E, Schreiber V, Mota R, Fuente T, Minguela A,**
495 **Parrilla P, de Murcia G, Almarza E, Aparicio P, and Menissier-de Murcia J.** PARP-2 deficiency affects
496 the survival of CD4+CD8+ double-positive thymocytes. *EMBO J* 25: 4350-4360, 2006.
497 33. **Zheng SJ, Wang P, Tsabary G, and Chen YH.** Critical roles of TRAIL in hepatic cell death and
498 hepatic inflammation. *J Clin Invest* 113: 58-64, 2004.

499

500

Figures legends

Figure 1: The absence of PARP2 but not PARP1 protects mice from ConA induced-hepatitis. (A) Serum levels of serum AST and ALT in WT, *Parp1*$^{-/-}$, and *Parp2*$^{-/-}$ mice, 11 h after PBS (n = 4 to 6) or ConA injection (n =1 3 for WT, 8 for *Parp1*$^{-/-}$, and 24 for *Parp2*$^{-/-}$). (B) Representative images of H&E stained liver tissue sections, necrosis areas are outlined by the white dotted line. (C) Serum levels of ALT of WT or *Parp2*$^{-/-}$ mice 24 h after ConA treatment. (D) Levels of liver TNF-α, IFN-γ, IL-1β, and IL-4 transcripts from WT, *Parp1*$^{-/-}$, and *Parp2*$^{-/-}$ mice 11 h after ConA administration. (E) Serum levels of TNF-α, IFN-γ and IL-6 in WT and *Parp2*$^{-/-}$ mice, 11 h after PBS (n = 4 to 6) or ConA injection (n= 6 to 11). For the scatter plots, errors bars represent + SEM. (* #p < 0.05; ** ## p < 0.01; *** ### p < 0.001; ns: non-significant).

Figure 2: PARP2 deficiency results in a decrease in the number of liver iNKT cells. (A) Gating strategy used to analyze lymphocyte subpopulations (NKT, NK, T cells, B cells) and myeloid cells in the liver and spleen. The gating strategy for liver immune cells is presented. (B) Absolute number of liver immune cells. (C) Absolute number of T lymphocytes (CD3+ TCRVb+NK1.1-), CD4-positive cells (in black) and CD8-positive cells (in white). (D) Absolute number of NKT cells (CD3+ TCRVb+NK1.1-) in the liver (E) Representative dot plot showing NKT subsets in the liver (left panel) and absolute number of liver iNKT cells (corresponding to aGalCer+CD4+ and aGalCer+CD4- cells) (middle panel) and liver NKT DN-cells (aGalCer-CD4-) (right panel). (F) Representative dot plot showing liver NK-cell population (left part) and absolute number of liver NK cells (NK1.1+CD3-) (right panel). (G) Absolute number of liver B-lymphocytes (CD19+CD11b) and (H) myeloid

cells (GR1^{int}CD11b+ and GR1^{high}CD11b+). All suspensions of liver immune cells from non-treated mice, aged 5 or 10 to 12 weeks, were obtained from the livers of WT or *Parp2*$^{-/-}$ mice. Each dot in the graph represents the number of cells recovered from one liver. The line and error bars represent the mean +/- SEM. For the histograms, the errors bars represent + SD. (* #p < 0.05; ** ## p < 0.01; *** ### p < 0.001; ns: non-significant).

Figure 3: PARP2 deficiency does not affect ConA-induced liver-leucocyte recruitment or activation. (A) Absolute number of liver immune cells from WT or *Parp2*$^{-/-}$ adult mice, non-treated (Ctl) or treated with ConA. Immune cells were isolated 11 or 24 h after ConA treatment. (B) Absolute number of NKT-cells from the livers of WT or *Parp2*$^{-/-}$ mice at steady state (Ctl) or 11 h after ConA treatment. (C) Absolute number of lymphocytes: T cells, B cells, and NK cells (upper panel) and myeloid cells (lower part) from liver of WT or *Parp2*$^{-/-}$ mice at steady state or 11 h after ConA treatment. (D) Representation of the activation marker (CD69) of T-lymphocytes CD8+ (NK1.1-TCRVb+CD3+CD8+) in the liver of WT or *Parp2*$^{-/-}$ mice treated or not with ConA. The line and error bars represent the mean + SD (* #p < 0.05; ** ## p < 0.01; *** ### p < 0.001; ns: non-significant).

Figure 4: PARP2 deficiency results in a reduction in the number of iNKT cells in the spleen. (A) Number of splenocytes of non-treated WT and *Parp2*$^{-/-}$ mice, aged 5 (early adult mice) or 10 at 12 weeks (adult mice). (B) Percentage of T lymphocytes (CD3+), TCRVb+NK1.1-), (C) B- ymphocytes (CD19+CD11b-), (D) total NKT cells (CD3+TCRVb+NK1.1+) (left panel), and NKT subsets: iNKT (NKT, α-GalCer+) (midle panel) and NKT-DN (NKT, α-GalCer- CD4-) (right panel), (E) NK cells (CD3-NK1.1+)

551 determined by flow cytometry analysis from spleens of early-adult or adult WT and
552 *Parp2*$^{-/-}$ mice. Each dot in the graph represents the number of cells recovered from
553 one liver. The lines and error bars represent the mean +/- SEM. (* p <0.05; ** p <
554 0.01; *** p < 0.001; ns: non-significant).
555
556 **Figure 5: PARP2 deficiency results in a decreased number of CD4/CD8 DP and**
557 **SP cells as well as iNKT cells.** (A) Representative staining profiles of CD4 and CD8
558 single or double positive cells from the thymus of non-treated five-week-old WT or
559 *Parp2*$^{-/-}$ mice. (B) Graph showing total number and the number of $CD4^{+}CD8^{+}$ double
560 positive thymocytes. (C) Representative staining profile of αGalCer positive
561 thymocytes. (D) Representation of mature T-cell markers (CD3 and TCRVβ) of
562 αGalCer positive thymocytes. Each dot in the graph represent the number of cells
563 recovered from one liver. The lines and errors bars represent the mean +/- SEM. (*
564 p<0.05; ** p<0.01; *** p<0.001; ns: non-significant).
565
566 **Figure 6: *Parp2*$^{-/-}$ mice display an increased number of Ter119+-cells but not of**
567 **other mature or immature subsets.** (A) Gating strategy used to analyze bone
568 marrow immune cell subsets. (B) Absolute number of cells recovered from two
569 femurs of WT or *Parp2*$^{-/-}$ adult (10 at 12 weeks old) mice. (C) Absolute cell number
570 for each mature bone marrow immune cells subset: $Ter119^{+}$, $CD19^{+}$, $CD3^{+}$,
571 $GR1^{high}CD11b^{+}$, and $GR1^{int}CD11b^{+}$. (D) Absolute number of immature Lin- bone
572 marrow immune cells ($Ter119^{-}$ $CD19^{-}$ $CD3^{-}$ $GR1^{-}$ $CD11b^{-}$) (left panel) and the specific
573 MP (Lin-ckit+Sca-) and LSK (Lin-ckit+Sca+) subsets (right panel). Each dot in the
574 graph represents the number of cells recovered from one liver. The lines and errors

575 bars represent the mean +/- SEM. (* $p<0.05$; ** $p<0.01$; *** $p<0.001$; ns: non-
576 significant).

Figure 1

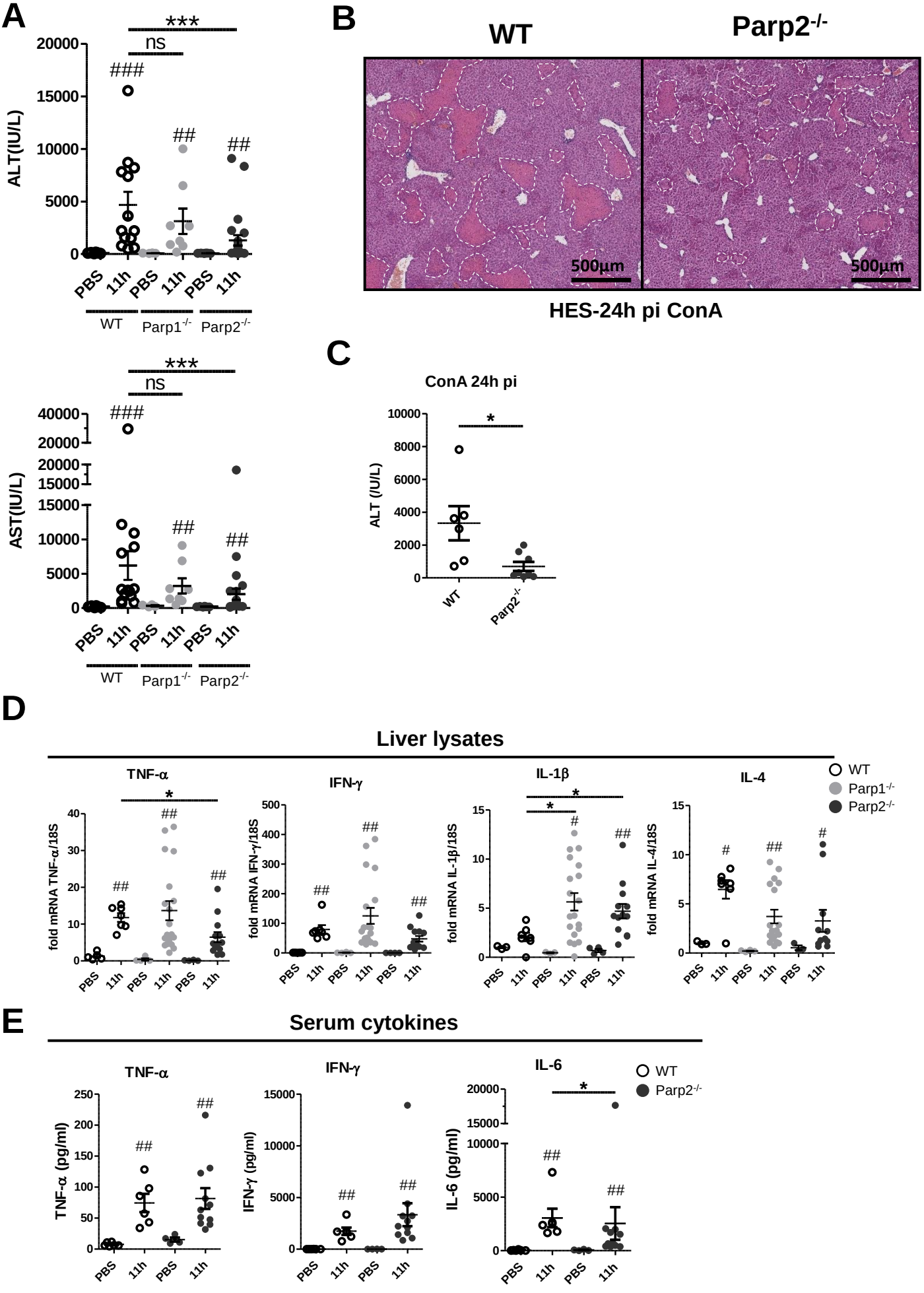
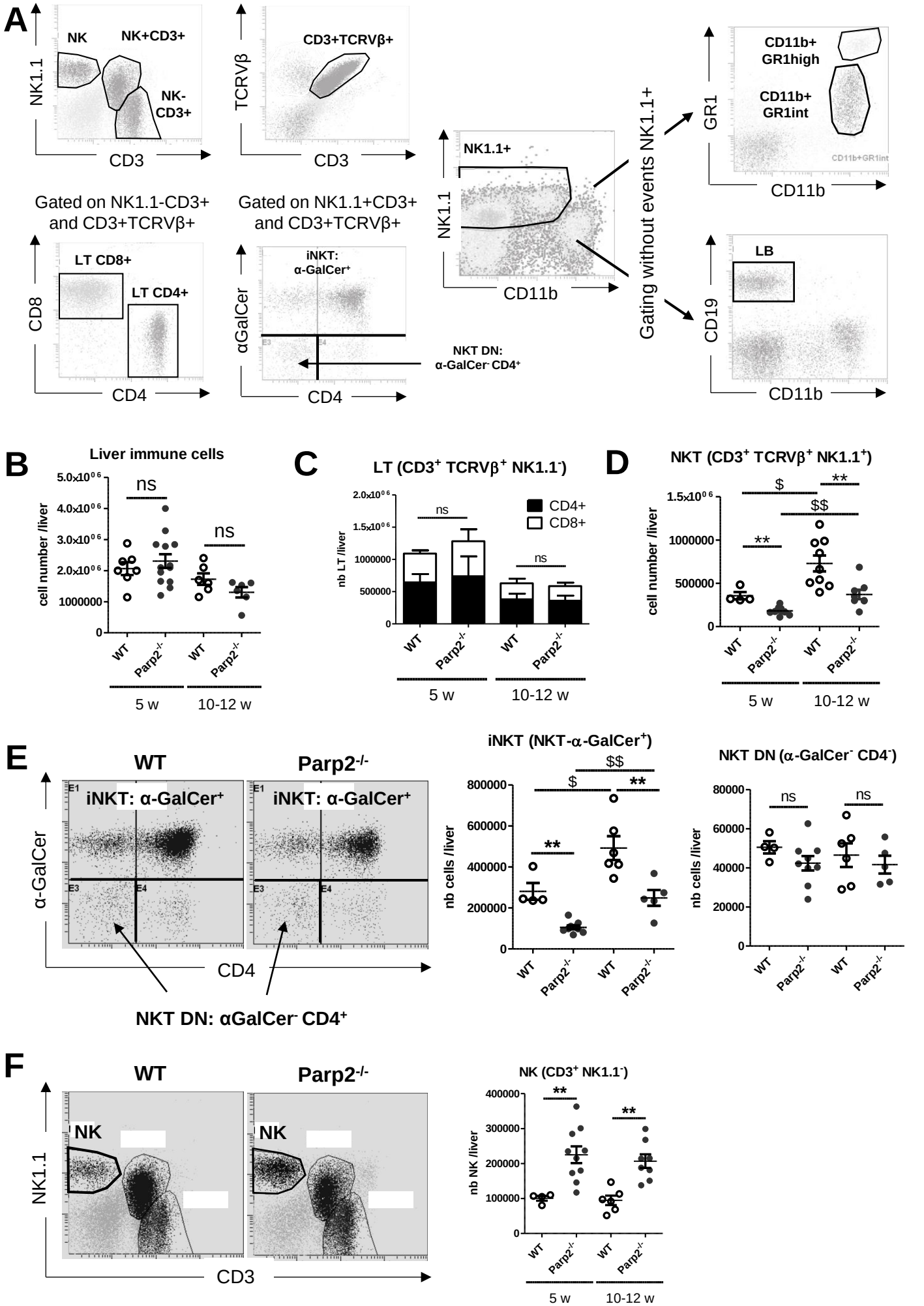
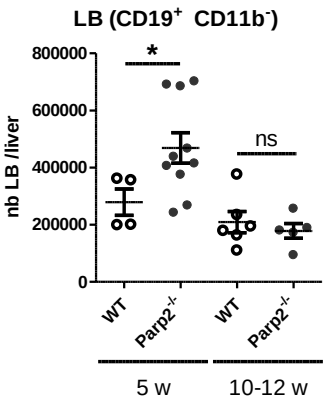

A
ALT(IU/L)
AST(IU/L)
***
ns
###
##
PBS
11h
WT
Parp1-/-
Parp2-/-
B
WT
Parp2-/-
500µm
HES-24h pi ConA
C
ConA 24h pi
ALT (/U/L)
*
D
Liver lysates
TNF-α
IFN-γ
IL-1β
IL-4
fold mRNA TNF-α/18S
fold mRNA IFN-γ/18S
fold mRNA IL-1β/18S
fold mRNA IL-4/18S
E
Serum cytokines
TNF-α (pg/ml)
IFN-γ (pg/ml)
IL-6 (pg/ml)
IL-6

Figure 2


A
NK
NK+CD3+
NK-CD3+
NK1.1
CD3
CD3+TCRVβ+
TCRVβ
CD3
NK1.1+
CD11b
Gating without events NK1.1+
CD11b+ GR1high
CD11b+ GR1int
GR1
CD11b
LB
CD19
CD11b
Gated on NK1.1-CD3+ and CD3+TCRVβ+
LT CD8+
LT CD4+
CD8
CD4
Gated on NK1.1+CD3+ and CD3+TCRVβ+
iNKT: α-GalCer+
αGalCer
CD4
NKT DN: α-GalCer- CD4+
B
Liver immune cells
cell number /liver
ns
ns
WT
Parp2-/-
WT
Parp2-/-
5 w
10-12 w
C
LT (CD3+ TCRVβ+ NK1.1-)
nb LT /liver
CD4+
CD8+
ns
ns
WT
Parp2-/-
WT
Parp2-/-
5 w
10-12 w
D
NKT (CD3+ TCRVβ+ NK1.1+)
cell number /liver
$
**
$$
**
WT
Parp2-/-
WT
Parp2-/-
5 w
10-12 w
E
WT
Parp2-/-
iNKT: α-GalCer+
iNKT: α-GalCer+
α-GalCer
CD4
NKT DN: αGalCer- CD4+
iNKT (NKT-α-GalCer+)
nb cells /liver
$$
$
**
**
NKT DN (α-GalCer- CD4-)
nb cells /liver
ns
ns
F
WT
Parp2-/-
NK
NK
NK1.1
CD3
NK (CD3+ NK1.1-)
nb NK /liver
**
**
5 w
10-12 w

G


LB (CD19+ CD11b-)
nb LB /liver
800000
600000
400000
200000
0
*
ns
WT
Parp2-/-
WT
Parp2-/-
5 w
10-12 w

H

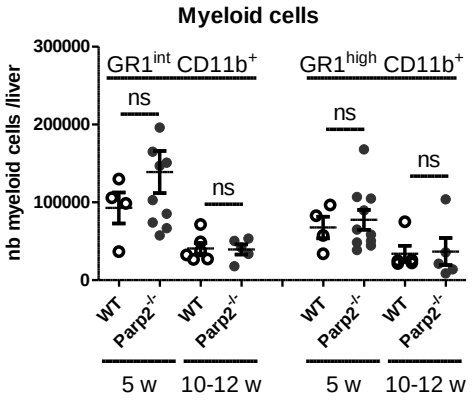

Myeloid cells
nb myeloid cells /liver
300000
200000
100000
0
GR1int CD11b+
GR1high CD11b+
ns
ns
ns
ns
WT
Parp2-/-
WT
Parp2-/-
WT
Parp2-/-
WT
Parp2-/-
5 w
10-12 w
5 w
10-12 w

Figure 3

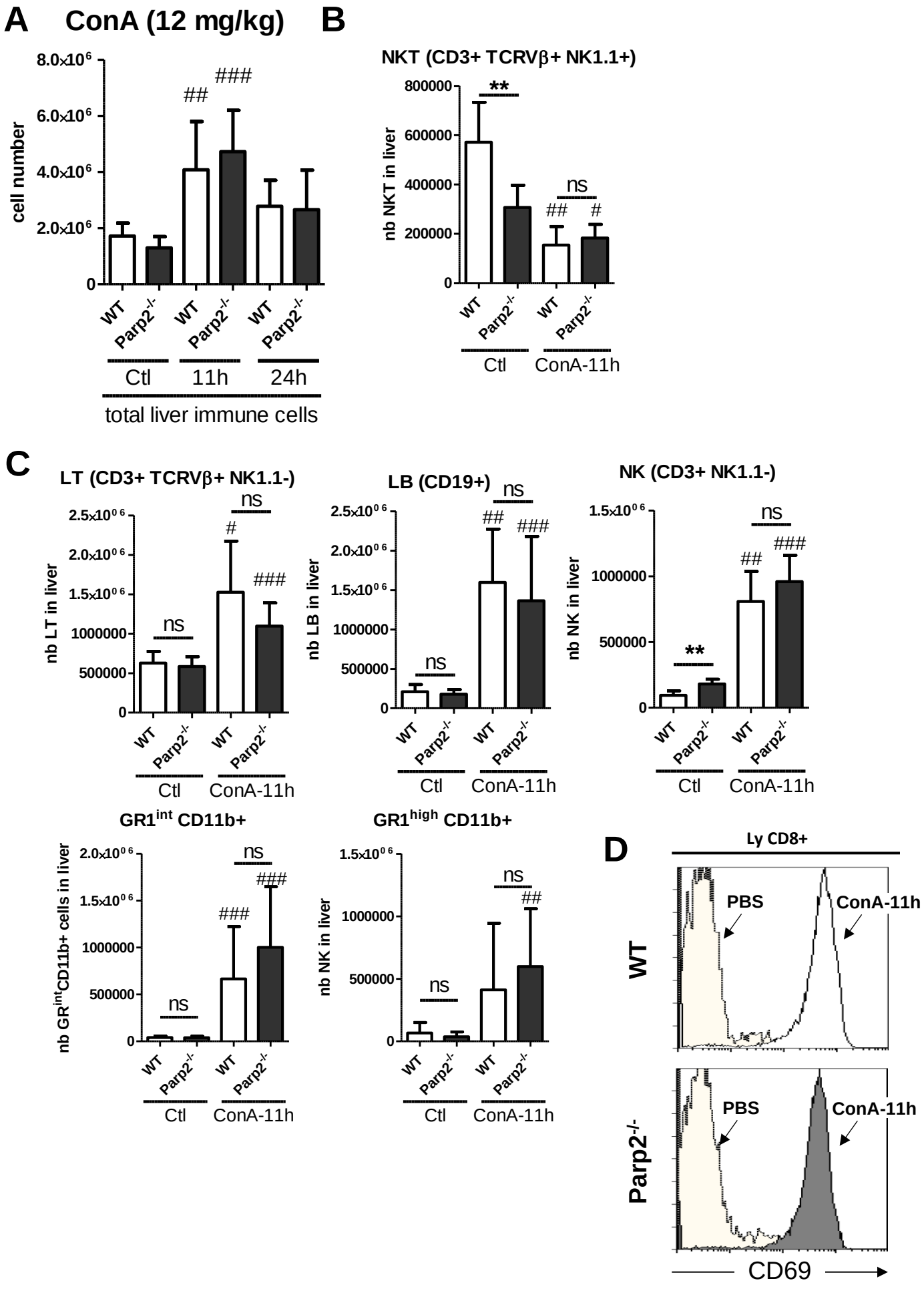

A
ConA (12 mg/kg)
cell number
8.0x10^6
6.0x10^6
4.0x10^6
2.0x10^6
0
##
###
WT
Parp2-/-
Ctl
11h
24h
total liver immune cells
B
NKT (CD3+ TCRVβ+ NK1.1+)
nb NKT in liver
800000
600000
400000
200000
0
**
ns
##
#
Ctl
ConA-11h
C
LT (CD3+ TCRVβ+ NK1.1-)
nb LT in liver
2.5x10^06
2.0x10^06
1.5x10^06
1000000
500000
LB (CD19+)
nb LB in liver
NK (CD3+ NK1.1-)
nb NK in liver
1.5x10^06
GR1int CD11b+
nb GRintCD11b+ cells in liver
GR1high CD11b+
nb NK in liver
D
Ly CD8+
PBS
ConA-11h
WT
Parp2-/-
CD69

Figure 4

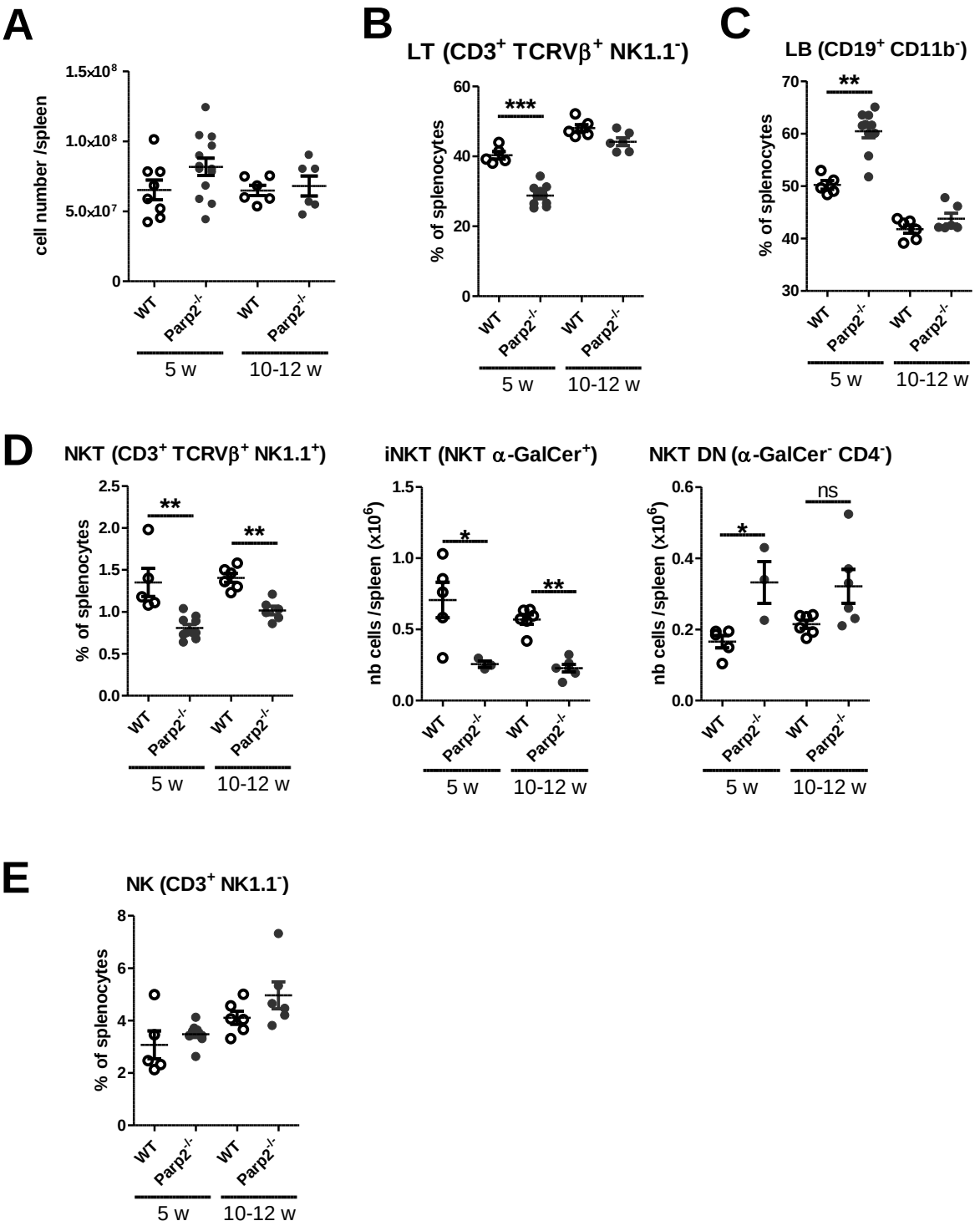

A
cell number /spleen
1.5x10^8
1.0x10^8
5.0x10^7
0
WT
Parp2-/-
WT
Parp2-/-
5 w
10-12 w
B
LT (CD3+ TCRVβ+ NK1.1-)
% of splenocytes
60
40
20
0
***
WT
Parp2-/-
WT
Parp2-/-
5 w
10-12 w
C
LB (CD19+ CD11b-)
% of splenocytes
70
60
50
40
30
**
WT
Parp2-/-
WT
Parp2-/-
5 w
10-12 w
D
NKT (CD3+ TCRVβ+ NK1.1+)
% of splenocytes
2.5
2.0
1.5
1.0
0.5
0.0
**
**
WT
Parp2-/-
WT
Parp2-/-
5 w
10-12 w
iNKT (NKT α-GalCer+)
nb cells /spleen (x10^6)
1.5
1.0
0.5
0.0
*
**
WT
Parp2-/-
WT
Parp2-/-
5 w
10-12 w
NKT DN (α-GalCer- CD4-)
nb cells /spleen (x10^6)
0.6
0.4
0.2
0.0
*
ns
WT
Parp2-/-
WT
Parp2-/-
5 w
10-12 w
E
NK (CD3+ NK1.1-)
% of splenocytes
8
6
4
2
0
WT
Parp2-/-
WT
Parp2-/-
5 w
10-12 w

Figure 5

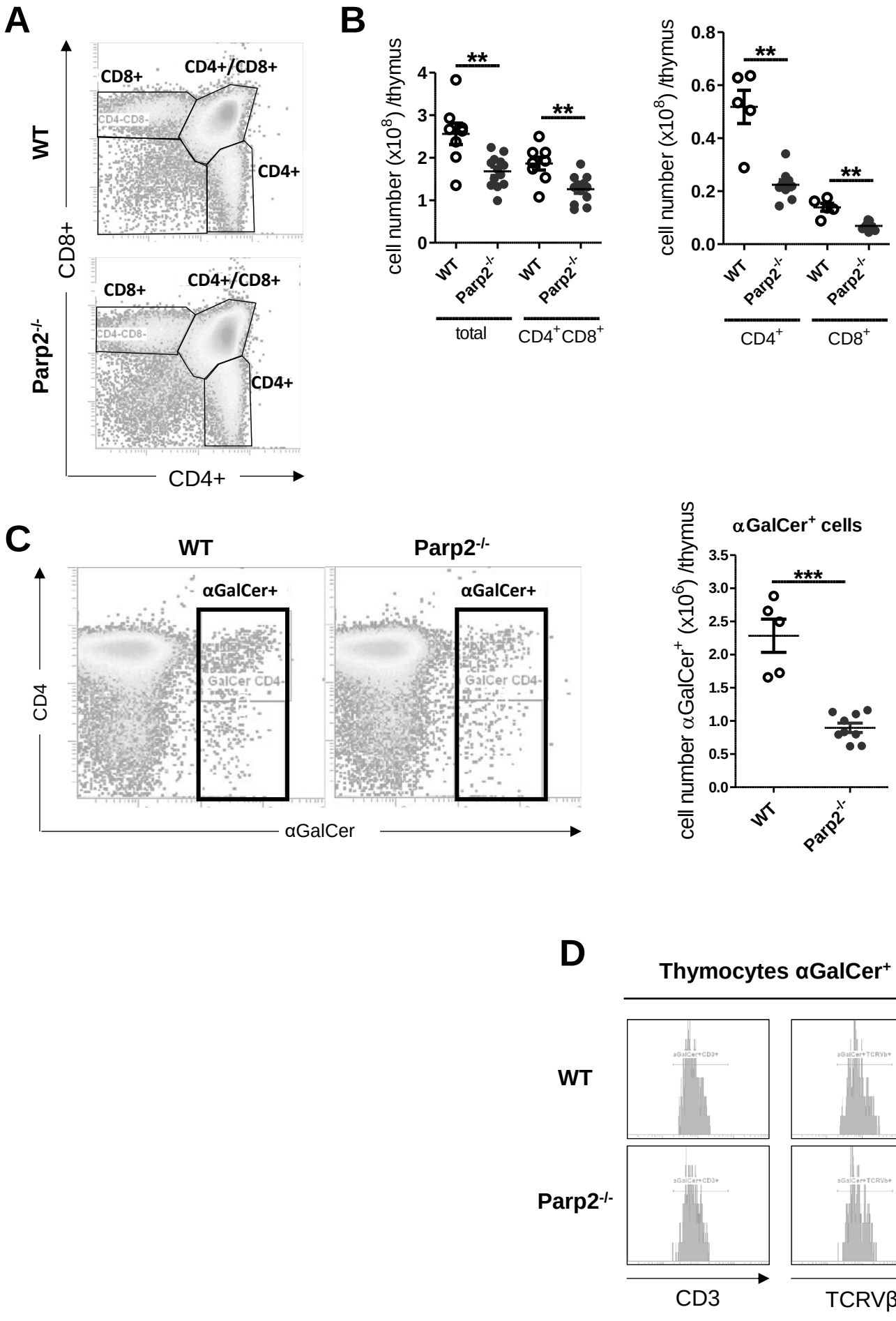
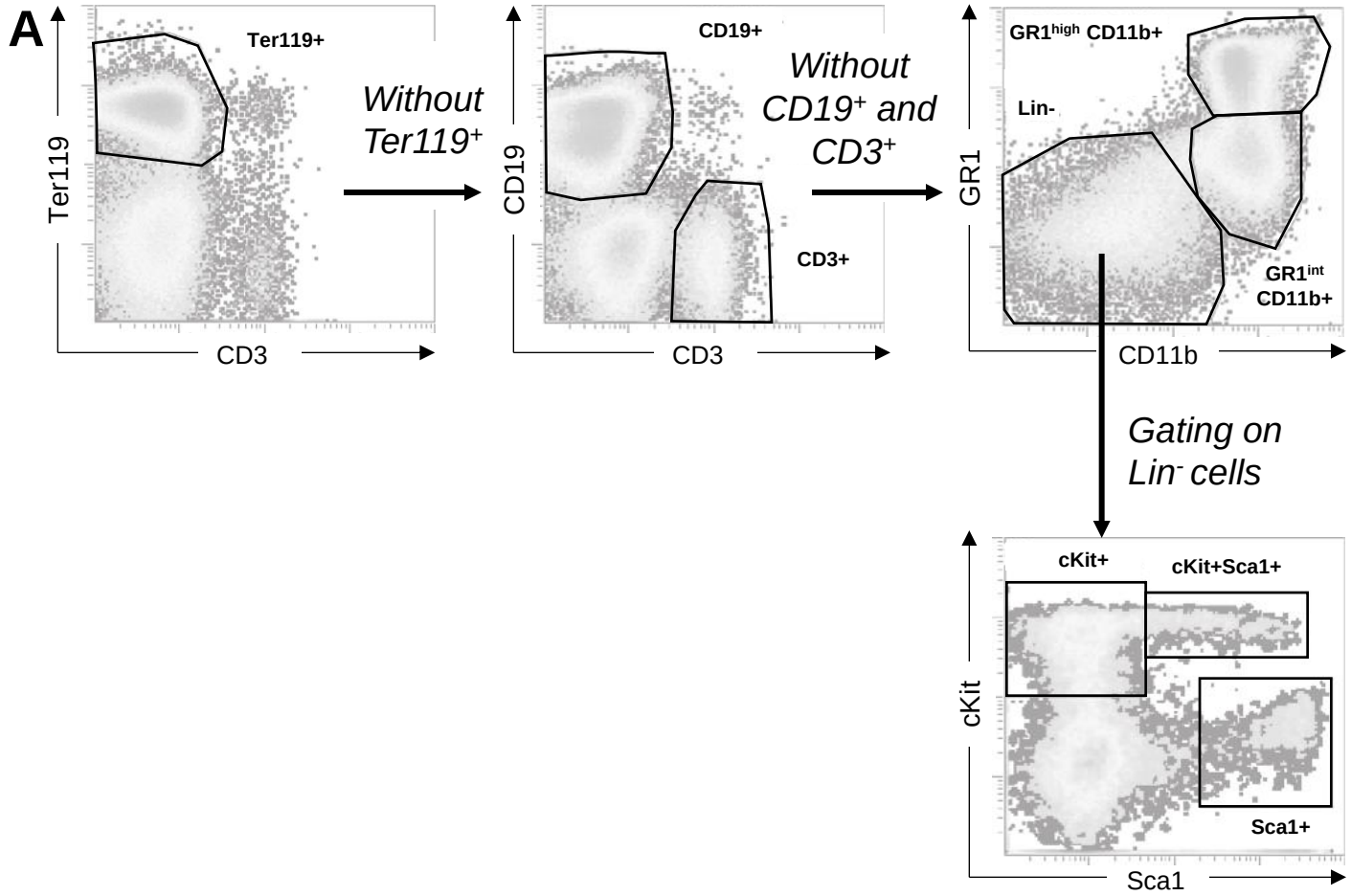
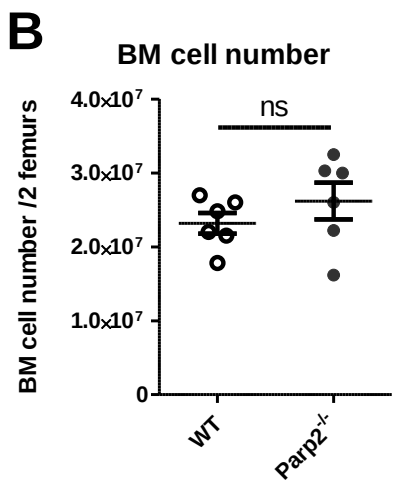
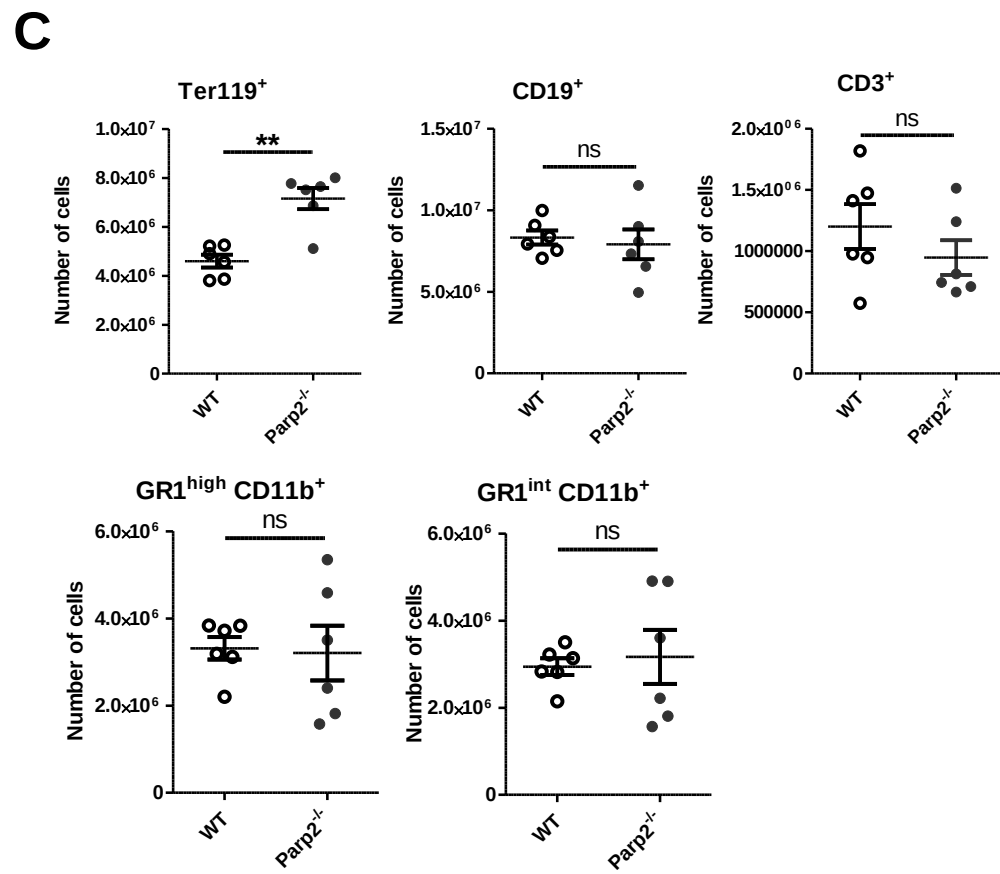

A
WT
Parp2-/-
CD8+
CD4+
CD4+/CD8+
CD4-CD8-
B
cell number (x10^8) /thymus
**
WT
Parp2-/-
total
CD4+CD8+
cell number (x10^8) /thymus
CD4+
CD8+
C
WT
Parp2-/-
αGalCer+
GalCer CD4-
CD4
αGalCer
αGalCer+ cells
cell number αGalCer+ (x10^6) /thymus
***
D
Thymocytes αGalCer+
WT
Parp2-/-
CD3
TCRVβ

Figure 6


A
Ter119+
Ter119
CD3
Without Ter119+
CD19+
CD19
CD3+
CD3
Without CD19+ and CD3+
GR1high CD11b+
Lin-
GR1int CD11b+
GR1
CD11b
Gating on Lin- cells
cKit+
cKit+Sca1+
Sca1+
cKit
Sca1


B
BM cell number
BM cell number /2 femurs
4.0x10^7
3.0x10^7
2.0x10^7
1.0x10^7
0
ns
WT
Parp2-/-


C
Ter119+
CD19+
CD3+
GR1high CD11b+
GR1int CD11b+
Number of cells
1.0x10^7
8.0x10^6
6.0x10^6
4.0x10^6
2.0x10^6
0
1.5x10^7
5.0x10^6
2.0x10^06
1.5x10^06
1000000
500000
**
ns
WT
Parp2-/-

D

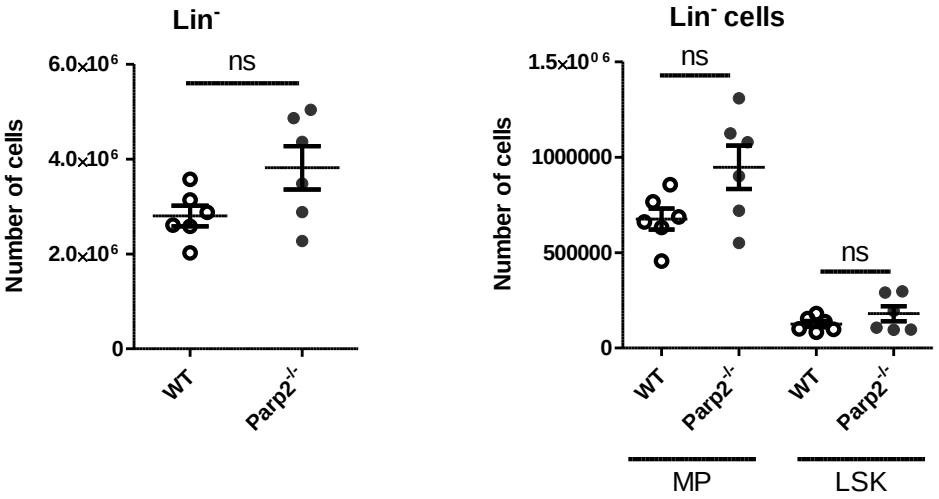

Lin-
Number of cells
6.0x10^6
4.0x10^6
2.0x10^6
0
ns
WT
Parp2-/-
Lin- cells
1.5x10^0 6
1000000
500000
0
ns
ns
WT
Parp2-/-
WT
Parp2-/-
MP
LSK

Table 1. Sequence of primers used for qPCR

Gene	Forward	Reverse
Mouse 18S	5′-CGCCGCTAGAGGTGAAATTC-3′	5′-TTGGCAAATGCTTTCGCTC-3′
Mouse TNFα	5′-TAGCTCCCAGAAAAGCAAGC-3′	5′-TTTTCTGGAGGGAGATGTGG-3′
Mouse IFN-γ	5’AGGTCAACAACCCACAGGTC3’	5’ATCAGCAGCGACTCCTTTTC3’
Mouse IL-1β	5’-GAAGAAGTGCCCATCCTCTG-3’	5’-AGCTCATATGGGTCCGACAG-3’
Mouse IL-4	5’-GGCTTCCAAGGTGCTTGG-3’	5’-GGACTTGGACTCATTCATGG-3’